

## Measurement at n\_TOF of the $^{237}\text{Np}(n,\gamma)$ and $^{240}\text{Pu}(n,\gamma)$ Cross Sections for the Transmutation of Nuclear Waste

C. Guerrero<sup>31</sup>, U. Abbondanno<sup>20</sup>, G. Aerts<sup>7</sup>, H. Álvarez<sup>25</sup>, F. Alvarez-Velarde<sup>31</sup>, S. Andriamonje<sup>7</sup>, J. Andrzejewski<sup>26</sup>, P. Assimakopoulos<sup>16</sup>, L. Audouin<sup>12</sup>, G. Badurek<sup>1</sup>, P. Baumann<sup>10</sup>, F. Bečvář<sup>6</sup>, E. Berthoumieux<sup>7</sup>, F. Calviño<sup>34</sup>, D. Cano-Ott<sup>31</sup>, R. Capote<sup>336</sup>, A. Camillo de Albornoz<sup>27</sup>, P. Cennini<sup>37</sup>, V. Chepell<sup>28</sup>, E. Chiaveri<sup>37</sup>, N. Colonna<sup>19</sup>, G. Cortes<sup>33</sup>, A. Couture<sup>41</sup>, J. Cox<sup>41</sup>, M. Dahlfors<sup>37</sup>, S. David<sup>9</sup>, I. Dillmann<sup>12</sup>, R. Dolfini<sup>23</sup>, C. Domingo-Pardo<sup>32</sup>, W. Dridi<sup>7</sup>, I. Duran<sup>35</sup>, C. Eleftheriadis<sup>13</sup>, L. Ferrant<sup>9</sup>, A. Ferrant<sup>9</sup>, R. Ferreira-Marques<sup>28</sup>, L. Fitzpatrick<sup>37</sup>, H. Fraiss-Koelbl<sup>3</sup>, K. Fujii<sup>20</sup>, W. Furman<sup>30</sup>, I. Goncalves<sup>28</sup>, R. Gallino<sup>22</sup>, E. Gonzalez-Romero<sup>31</sup>, A. Goverdovski<sup>29</sup>, F. Gramigna<sup>18</sup>, E. Griesmayer<sup>3</sup>, F. Gunsing<sup>7</sup>, B. Haas<sup>8</sup>, R. Haight<sup>39</sup>, M. Heil<sup>12</sup>, A. Herrera-Martinez<sup>37</sup>, M. Igashira<sup>25</sup>, S. Isaev<sup>9</sup>, E. Jericha<sup>1</sup>, Y. Kadi<sup>37</sup>, F. Käppeler<sup>12</sup>, D. Karamanis<sup>16</sup>, D. Karadimos<sup>16</sup>, M. Kerveno<sup>10</sup>, V. Ketterov<sup>2937</sup>, P. Koehler<sup>40</sup>, V. Kononov<sup>3037</sup>, E. Kossionides<sup>15</sup>, M. Kríčka<sup>6</sup>, C. Lamboudis<sup>13</sup>, H. Leeb<sup>1</sup>, A. Lindote<sup>28</sup>, I. Lopes<sup>28</sup>, M. Lozano<sup>36</sup>, S. Lukic<sup>10</sup>, J. Marganic<sup>26</sup>, L. Marques<sup>27</sup>, T. Martinez<sup>31</sup>, S. Marrone<sup>19</sup>, C. Massimi<sup>21</sup>, P. Mastinu<sup>18</sup>, A. Mengoni<sup>337</sup>, P.M. Milazzo<sup>20</sup>, C. Moreau<sup>20</sup>, M. Mosconi<sup>12</sup>, F. Neves<sup>28</sup>, H. Oberhammer<sup>1</sup>, S. O'Brien<sup>41</sup>, M. Oshima<sup>24</sup>, J. Pancin<sup>7</sup>, C. Papachristodoulou<sup>16</sup>, C. Papadopoulos<sup>14</sup>, C. Parada<sup>35</sup>, N. Patronis<sup>16</sup>, A. Pavlik<sup>2</sup>, P. Pavlopoulos<sup>11</sup>, L. Perrot<sup>7</sup>, R. Plag<sup>12</sup>, A. Plompen<sup>5</sup>, A. Plukis<sup>7</sup>, A. Poch<sup>33</sup>, C. Pretel<sup>33</sup>, J. Quesada<sup>36</sup>, T. Rauscher<sup>38</sup>, R. Reifarth<sup>39</sup>, M. Rosetti<sup>17</sup>, C. Rubbia<sup>23</sup>, G. Rudolf<sup>40</sup>, P. Rullhusen<sup>5</sup>, J. Salgado<sup>27</sup>, L. Sarchiapone<sup>37</sup>, I. Savvidis<sup>13</sup>, C. Stephan<sup>9</sup>, G. Tagliente<sup>19</sup>, J.L. Tain<sup>32</sup>, L. Tassan-Got<sup>3</sup>, L. Tavora<sup>27</sup>, R. Terlizzi<sup>19</sup>, G. Vannini<sup>21</sup>, P. Vaz<sup>27</sup>, A. Ventura<sup>17</sup>, D. Villamarin<sup>31</sup>, M.C. Vicente<sup>31</sup>, V. Vlachoudis<sup>37</sup>, R. Vlastou<sup>14</sup>, F. Voss<sup>12</sup>, S. Walter<sup>12</sup>, H. Wendler<sup>37</sup>, M. Wiescher<sup>41</sup> and K. Wisshak<sup>12</sup>

### The n\_TOF Collaboration

- <sup>1</sup>Atominstüt der Österreichischen Universitäten, Technische Universität Wien, Austria,  
<sup>2</sup>Institut für Isotopenforschung und Kernphysik, Universität Wien, Austria,  
<sup>3</sup>International Atomic Energy Agency (IAEA), Nuclear Data Section, Vienna, Austria  
<sup>4</sup>Fachhochschule Wiener-Neustadt, Wiener-Neustadt, Austria,  
<sup>5</sup>CEC-JRC-IRMM, Geel, Belgium,  
<sup>6</sup>Charles University, Prague, Czech Republic,  
<sup>7</sup>CEA/Saclay - DSM, Gif-sur-Yvette, France,  
<sup>8</sup>Centre National de la Recherche Scientifique/IN2P3 - CENBG, Bordeaux, France,  
<sup>9</sup>Centre National de la Recherche Scientifique/IN2P3 - IPN, Orsay, France,  
<sup>10</sup>Centre National de la Recherche Scientifique/IN2P3 - IReS, Strasbourg, France,  
<sup>11</sup>Pôle Universitaire Léonard de Vinci, Paris La Défense, France,  
<sup>12</sup>Forschungszentrum Karlsruhe GmbH (FZK), Institut für Kernphysik, Germany,  
<sup>13</sup>Aristotle University of Thessaloniki, Greece,  
<sup>14</sup>National Technical University of Athens, Greece  
<sup>15</sup>NCSR, Athens, Greece,  
<sup>16</sup>University of Ioannina, Greece,  
<sup>17</sup>ENEA, Bologna, Italy,  
<sup>18</sup>Istituto Nazionale di Fisica Nucleare (INFN), Laboratori Nazionali di Legnaro, Italy,  
<sup>19</sup>Istituto Nazionale di Fisica Nucleare, Bari, Italy,  
<sup>20</sup>Istituto Nazionale di Fisica Nucleare, Trieste, Italy,  
<sup>21</sup>Dipartimento di Fisica, Università di Bologna, and Sezione INFN di Bologna, Italy,  
<sup>22</sup>Dipartimento di Fisica, Università di Torino and Sezione INFN di Torino, Italy,  
<sup>23</sup>Università degli Studi Pavia, Pavia, Italy,  
<sup>24</sup>Japan Atomic Energy Research Institute, Tokai-mura, Japan,  
<sup>25</sup>Tokyo Institute of Technology, Tokyo, Japan,  
<sup>26</sup>University of Lodz, Lodz, Poland  
<sup>27</sup>Instituto Tecnológico e Nuclear (ITN), Lisbon, Portugal,  
<sup>28</sup>LIP - Coimbra & Departamento de Física da Universidade de Coimbra, Portugal,  
<sup>29</sup>Institute of Physics and Power Engineering, Kaluga region, Obninsk, Russia,  
<sup>30</sup>Joint Institute for Nuclear Research, Frank Laboratory of Neutron Physics, Dubna, Russia,  
<sup>31</sup>Centro de Investigaciones Energeticas Medioambientales y Tecnológicas, Madrid, Spain,  
<sup>32</sup>Istituto de Física Corpuscular, CSIC-Universidad de Valencia, Spain,  
<sup>33</sup>Universitat Politècnica de Catalunya, Barcelona, Spain,

<sup>34</sup>Universidad Politecnica de Madrid, Spain,

<sup>35</sup>Universidade de Santiago de Compostela, Spain,

<sup>36</sup>Universidad de Sevilla, Spain,

<sup>37</sup>CERN, Geneva, Switzerland,

<sup>38</sup>Department of Physics and Astronomy - University of Basel, Basel, Switzerland,

<sup>39</sup>Los Alamos National Laboratory, New Mexico, USA,

<sup>40</sup>Oak Ridge National Laboratory, Physics Division, Oak Ridge, USA,

<sup>41</sup>University of Notre Dame, Notre Dame, USA,

## Abstract

The final design, safety assessment and precise performance analysis of transmutation devices such as Accelerator Driven Systems (ADS) or Fast Critical Reactors, need accurate and reliable nuclear data. The cross sections of <sup>237</sup>Np and <sup>240</sup>Pu have been measured in 2004 at n\_TOF with good accuracy due to a combination of features unique in the world: high instantaneous neutron fluence and excellent energy resolution of the n\_TOF facility [1], innovative Data Acquisition System based on flash ADCs and the use of a high performance BaF<sub>2</sub> Total Absorption Calorimeter as a detection device.

**KEYWORDS:** nuclear data, neutron capture, cross sections, total absorption calorimeter, Monte Carlo simulation, neptunium, plutonium.

## 1. Introduction

The transmutation has been proposed as a way to reduce substantially (by a factor of 1/100 or more) the radiotoxicity inventory of the long lived component of the nuclear waste, mainly the trans-uranium actinides. Actinide transmutation takes place by fission in nuclear systems like critical reactors or subcritical Accelerator Driven Systems (ADS). Most of the scenarios consider the use of fast neutron energy spectra and fuels highly enriched in high mass trans-uranium actinides. The detailed engineering designs, safety evaluations and the detailed performance assessment of dedicated transmutation ADSs and critical reactors require more precise and complete basic nuclear data [2]. Of crucial importance is the composition of the fuels proposed, with a large concentration of minor actinides (MA) and high mass plutonium isotopes.

The transmutation of <sup>237</sup>Np plays an important role because of two main reasons. First, it has the largest capture ratio after <sup>239</sup>Pu in a typical ADS core loaded with a fuel highly enriched in MA. Second, Np is the actinide element presenting the highest leakage probability from a deep underground repository. The case of <sup>240</sup>Pu has also two main implications. First, <sup>240</sup>Pu is the second most abundant isotope (after <sup>239</sup>Pu) in the irradiated fuel discharged from a commercial Nuclear Power Plant. Second, depending on the fuel cycle (open or closed) <sup>240</sup>Pu can be the most abundant Pu isotope in the composition of the fuel for an ADS.

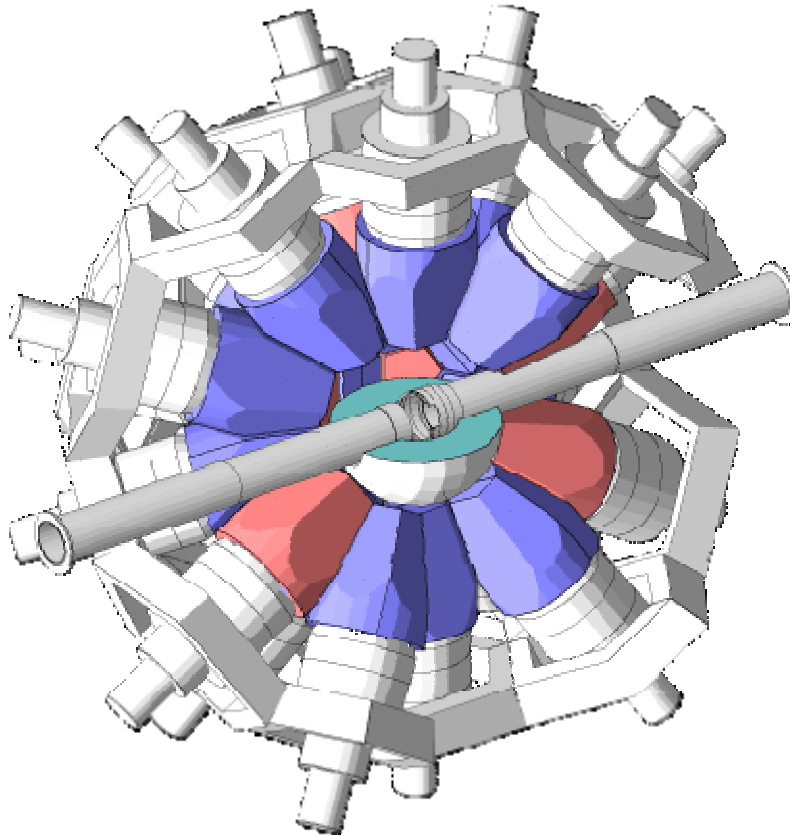
## 2. Measurement and Experimental Setup

Isotopically enriched targets of minor actinides are available typically in amounts ranging from 1-100 mg. Even for such small values the activity of the samples adds major difficulties to both to the experimental techniques and the radioprotection aspects.

The targets of  $^{237}\text{Np}$  (43.3 mg, 1.29 MBq) and  $^{240}\text{Pu}$  (51.2mg, 458 MBq) used in the measurements were assembled as follows: the radioactive material was sandwiched by two thin Al layers (total mass < 75 mg) and canned inside a 0.35 mm thick Ti canning with ISO 2919 certification (requested by the safety regulations at CERN). Their isotopic purity has been determined by  $\gamma$ -ray spectrometry and was better than 99% for  $^{237}\text{Np}$  and about 90% for  $^{240}\text{Pu}$  (with a 10% contamination of  $^{239}\text{Pu}$ ).

The neutron beam was 4 cm in diameter with an instantaneous fluence of  $\sim 10^5$  neutrons/cm<sup>2</sup>/pulse in the neutron energy range between 0.1 eV and 1 MeV. During the measurements, the repetition rate of the CERN proton synchrotron (PS) was on average 3 – 4 proton pulses for a PS supercycle of 16.4 s. The resolution in neutron energy at the 185 m flight path was a few times  $10^{-4}$  in the energy range of interest.

**Figure 1:** Geometry of the n\_TOF Total Absorption Calorimeter (TAC) as it is defined in the GEANT4 Monte Carlo simulation code.



The capture cross section measurements at n\_TOF were performed relative to the standard capture cross section of  $^{197}\text{Au}(n,\gamma)$ . Independent and highly accurate monitors were used permanently for a proper normalization between the  $^{197}\text{Au}(n,\gamma)$  yield and the measured data [3].

The Data Acquisition system (DAQ) comprised 54 channels of high performance flash ADCs [4-5]. Each channel has 8 Mbytes memory and was operated at a sampling rate of 500 MSamples/s, thus allowing to record the full detector history for the neutron energy range

between 0.3 eV and 20 GeV. After zero suppression and data formatting, the raw data are sent to CERN's massive storage facility CASTOR via several Gigabit links [6]. In parallel, especially designed pulse shape analysis routines are run on a PC farm and extract from the digitized detector signals the necessary information for further data analysis.

The n\_TOF DAQ offers unique features such as an extremely low dead time (<10 ns) as well as good signal analysis and pileup discrimination, resulting in an excellent control of the systematic uncertainties associated with the detector. The quality of the reconstruction of capture events in the sample have been discussed already in [7].

The neutron capture detection system consists of a segmented Total Absorption Calorimeter made of 40 BaF<sub>2</sub> crystals with <sup>10</sup>B loaded carbon fiber capsules, which is placed at 185 m flight path from the spallation source. The TAC has a nearly 100% detection efficiency for electromagnetic cascades (i.e. capture events) and a good energy resolution (14% at 662 keV and 6% at 6.1 MeV). The radioactive targets are placed at the geometric center of the TAC and are surrounded by a C<sub>12</sub>H<sub>20</sub>O<sub>4</sub>(<sup>6</sup>Li)<sub>2</sub> neutron absorber inside the inner hole of the TAC. The neutron absorber and the <sup>10</sup>B loaded carbon fiber capsules reduce the sensitivity for the detection of scattered neutrons, but do not reduce the overall detection efficiency (even though they lower the total absorption efficiency) and also help in attenuating the low energy component (10 - 100 keV) of the sample radioactivity.

Fig.1 shows a view of the experimental setup, as it is implemented in the code [8] used for the detailed MC simulations of the TAC. The performance of the TAC has been investigated both experimentally with calibration sources and via the reference <sup>197</sup>Au(n,γ) cross section, and by Monte Carlo simulations [9-10]. Furthermore, all sources of background have been measured and are being simulated for performing the background corrections necessary for an accurate capture cross section analysis.

### 3. Data Analysis and Preliminary Results

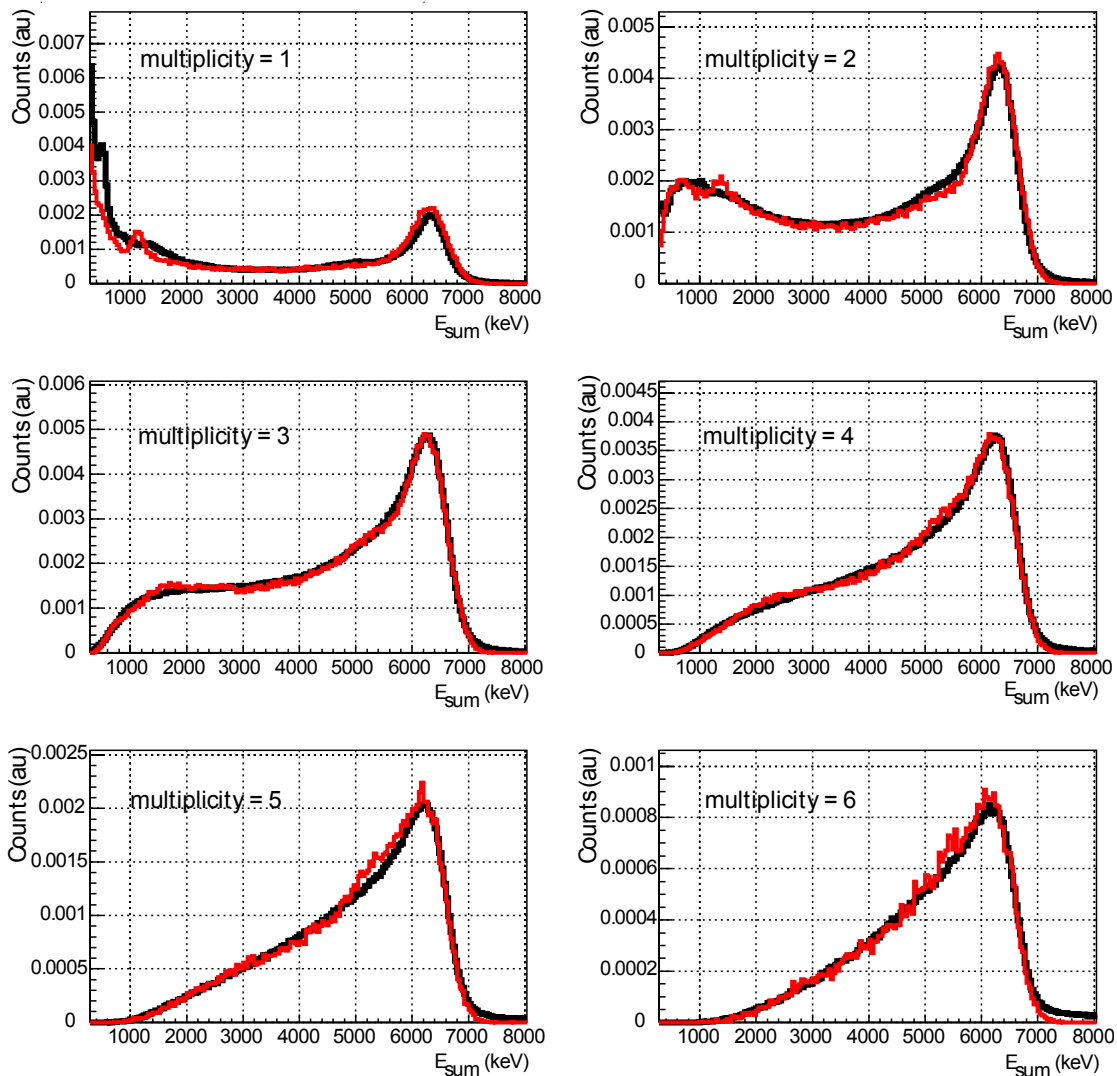
The major sources of systematic uncertainties associated to the data analysis have been investigated in detail.

#### 3.1 Detection Efficiency of the TAC

As mentioned previously, the TAC has nearly 100% efficiency for the detecting gamma ray cascades. However, in the real experiments the conditions were such that the best signal to noise (i.e. background) ratio in the data was found after selecting events with a multiplicity larger than 2 (i.e. number of individual crystals firing) and a total energy deposition in the TAC above 2 MeV. Under these conditions, the detection efficiency of the TAC drops down to 60% and shows a non negligible dependence on the particular electromagnetic (EM) de-excitation pattern of the gamma ray cascades. Thus, the detection efficiency of the TAC and its uncertainty has to be calculated for all <sup>197</sup>Au, <sup>237</sup>Np and <sup>240</sup>Pu samples. First, the energy deposition spectra for selected resonances in the three <sup>197</sup>Au, <sup>237</sup>Np and <sup>240</sup>Pu capture measurements were compared. Besides a degradation of the energy resolution as a function of the counting rate, the shape was found to be the same and nearly independent on the resonance spin. Then, the response of the TAC to realistic (EM) cascades was calculated by Monte Carlo simulation. For this purpose, a cascade

generator was built combining all the available information of the level schemes at low energies and completed with a statistical model for the de-excitation of the nucleus at higher excitation energies. The parameters of the model, mainly the E1, M1 and E2 gamma ray strength functions, had to be tuned in order to reproduce the data. Fig. 2 shows the comparison of the Monte Carlo simulated energy deposition spectra (in red) and the experimental data (in black) for various multiplicities. The reproduction of the data is excellent, thus allowing us to calculate the detection efficiency as a function of the multiplicity with an uncertainty below 3%. A similar situation was found for the  $^{237}\text{Np}$  and  $^{240}\text{Pu}$  samples.

**Figure 2:** Experimental and Monte Carlo simulated energy deposition spectra at different multiplicities for the 4.9 eV resonance in the  $^{197}\text{Au}(n,\gamma)$  reaction.



### 3.2 Normalization to the $^{197}\text{Au}(n,\gamma)$ cross section

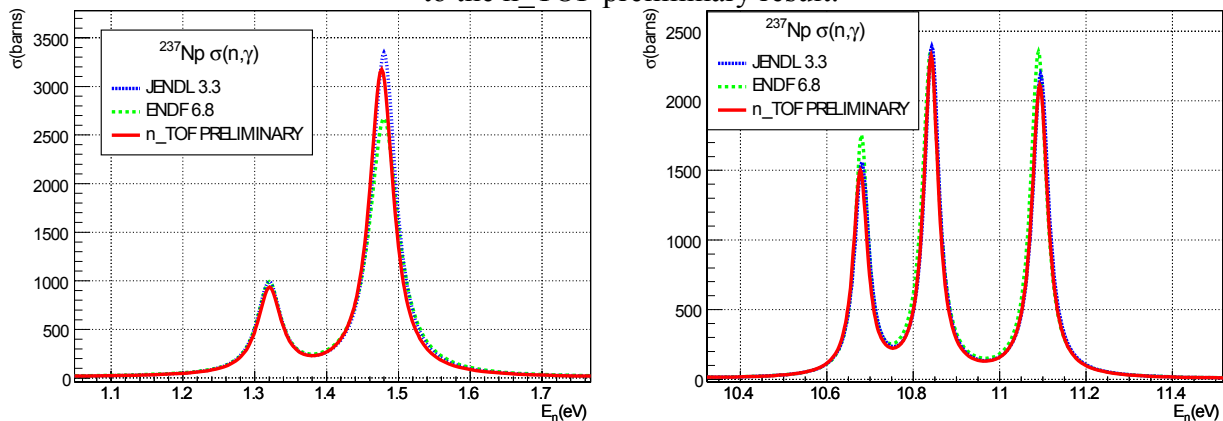
As it has been mentioned already, the neutron capture cross section measurements at n\_TOF are performed relative to the  $^{197}\text{Au}(n,\gamma)$  cross section. The shape of the neutron energy spectrum

at the sample position has been characterized accurately and is well known [1]. A 180 mg  $^{197}\text{Au}$  sample was irradiated in between the actinide measurements and the intensity of the neutron beam during the measurements was monitored with the Silicon Flux Monitor [3]. The non standard but well known 4.9 eV resonance integral in  $^{198}\text{Au}$  was used for normalizing the measurements. The uncertainty in its resonance parameters leads to a systematic uncertainty in the normalization below 1%, which has to be added to an uncertainty of 2% from possible geometric misalignment between the samples.

### 3.3 The neutron sensitivity of the TAC

Neutrons scattered at the sample can be captured by the TAC materials (mainly in the Ba isotopes) and misidentified as true capture events. Such a background, also called neutron sensitivity of the detector, can be harmful since it follows the resonant structure of the neutron elastic scattering cross section of the samples and can lead to an artificial broadening of the resonances. An upgraded version of the SAMMY code that allows one to define an arbitrary shape of the background has been used to estimate the effect of the neutron sensitivity [11]. A few resonances with particularly high  $\Gamma_n$  were selected in both Np and Pu data sets. The background spectra due to the neutron sensitivity were computed and included in the resonance analysis. Its effect on the resonance parameters is below 10%. In the final analysis, the neutron sensitivity will be included for every single resonance.

**Figure 3:** Comparison of the ENDF 6.8 and JENDL 3.3 evaluated  $^{237}\text{Np}$   $(n,\gamma)$  cross sections to the n\_TOF preliminary result.



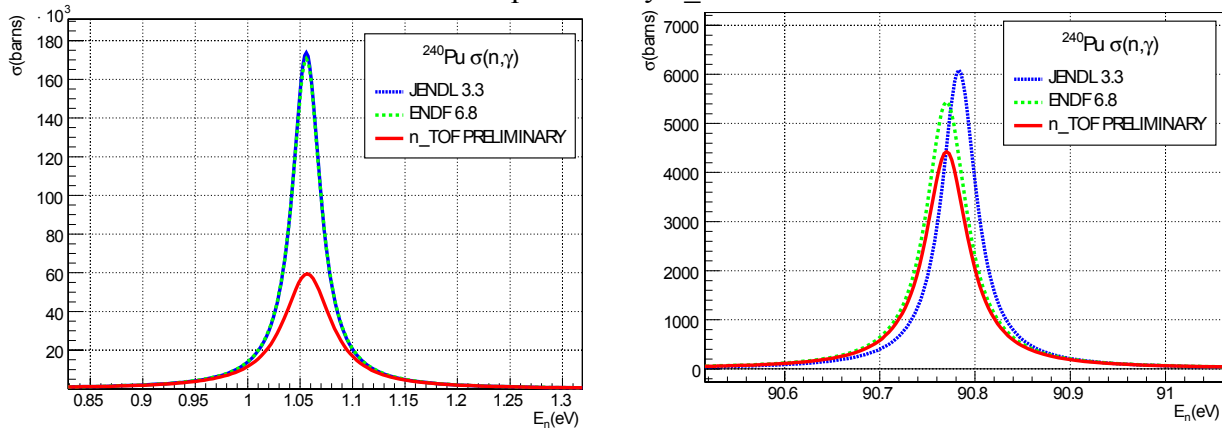
The Multilevel Breit Wigner formalism was used for facilitating a direct comparison to the evaluated resonance parameters found in the ENDFB 6.8 and JENDL 3.3 libraries. The final analysis is being performed however following the Reich Moore formalism. A large effort was made in developing the software tools that allowed the fast analysis of the data set in the entire energy range. In this way, the effect of the individual sources of systematic uncertainties can be computed systematically and used for the construction of the final covariance matrices.

The  $^{237}\text{Np}$  data have been analyzed up to 100 eV. Despite the high level density in  $^{238}\text{Np}$  and the effect of the Doppler broadening, most of the resonances described in the literature were

identified. Fig. 3 shows the comparison between the ENDF, JENDL and preliminary n\_TOF capture cross sections for the lowest lying and strongest resonances. It was found that there is a slightly better agreement with the JENDL 3.3 values than with the ENDFB 6.8 data. Indeed, the same trend has been observed over the entire energy range, including also the tabulated resonance energies. The n\_TOF resonance integrals are on average, 6% below the ENDFB 6.8 values and 3% below the JENDL 3.3 values. Such deviations are compatible with the 5% uncertainty in the mass of the  $^{237}\text{Np}$  sample used for the measurements.

The  $^{240}\text{Pu}$  data have been analyzed up to 1 keV. The  $^{239}\text{Pu}$  contamination was included in the analysis and treated by the SAMMY code as an isotopic impurity. Fig. 4 shows the comparison between the ENDF, JENDL, and the preliminary n\_TOF capture cross sections for the lowest lying and strongest resonances. It can be observed that there is a huge difference for the 1.06 eV resonance, where the n\_TOF value is 42% lower than the evaluations. A smaller but sizeable difference for the 90.7 eV resonance is also visible; here, the n\_TOF value is about 10% below the ENDF and JENDL evaluations.

**Figure 4:** Comparison of the ENDF 6.8 and JENDL 3.3 evaluations for  $^{240}\text{Pu}(n,\gamma)$  resonances with the preliminary n\_TOF results.



The average deviations for  $^{240}\text{Pu}$  are slightly larger than for the Np examples and could be partly attributed to the uncertainty of the  $^{240}\text{Pu}$  mass and its  $^{239}\text{Pu}$  impurity. The effect is under investigation and will be answered in the final analysis. However, no systematic effect has been found, which could explain the huge difference between the n\_TOF and evaluated cross section values at 1.06 eV. Thus, the preliminary conclusion is that indeed the 1.06 eV resonance is significantly weaker in the capture channel than reported previously.

#### 4. Summary and Conclusions

The neutron capture cross sections of  $^{237}\text{Np}$  and  $^{240}\text{Pu}$  have been measured at the n\_TOF facility at CERN. A high performance Total Absorption Calorimeter made of 40 BaF<sub>2</sub> crystals was used in the measurements. The uncertainty in the data is dominated by the 5% uncertainty in the mass of the samples. A preliminary resonance analysis of both data sets has been performed with the SAMMY code.

The results for the  $^{237}\text{Np}$  data up to 100 eV show good overall agreement with the ENDFB 6.8 and JENDL 3.3 evaluated cross sections. The n\_TOF resonance integrals are on average 6% below the ENDFB 6.8 values and 3% below the JENDL 3.3 values. Such deviations are compatible with the 5% uncertainty in the mass of the  $^{237}\text{Np}$  sample used. The resonance integrals obtained from the  $^{240}\text{Pu}$  data up to 1 keV are on average 9% below the ENDFB 6.8 and 7% below the JENDL 3.3 evaluated values. The deviations are slightly larger than for the Np case and could be partly attributed to the uncertainty of the  $^{240}\text{Pu}$  mass and its  $^{239}\text{Pu}$  impurity. However, the n\_TOF value for the 1.06 eV resonance is 42% below both evaluated libraries, hence in total disagreement. Possible sources of systematic uncertainties in the data are being investigated but such a large difference can hardly be accommodated. Taking into account that the agreement at higher energies is rather good, the preliminary conclusion is that indeed the 1.06 eV resonance is significantly weaker in the capture channel than reported previously.

## Acknowledgements

This work is part of the European Commission 5<sup>th</sup> Framework Programme project NTOF-ND-ADS under contract FIKW-CT-2000-00107. The authors would like to thank Nancy M. Larson (Nuclear Data Group – Oak Ridge National Laboratory) for her kindness, valuable help and the fast upgrading of the SAMMY code to their needs.

## References

- 1) U. Abbondano et al., "nTOF Performance Report", CERN/INTC-O-011, INTC-2002-037
- 2) G. Aliberti et al., "Impact of Nuclear Data Uncertainties on Transmutation of Actinides in Accelerator-Driven Assemblies", Nucl. Sci. Eng., **146**, 13 (2004).
- 3) S. Marrone et al., "A low background neutron flux monitor for the n\_TOF facility at CERN", Nucl. Instr. Meth. A, **517**, 389 (2004)
- 4) U. Abbondano et al., "The data acquisition system of the neutron time-of-flight facility n\_TOF at CERN", Nucl. Instr. Meth. A, **538**, 692 (2005).
- 5) <http://www.acqiris.com/>
- 6) <http://castor.web.cern.ch/castor/>
- 7) D. Cano-Ott et al., "Measurements at n\_TOF of the neutron capture cross section of minor actinides relevant to the transmutation of nuclear waste", Proc. Int. Conf. on Nuclear Data for Science and Technology, Santa Fe, USA, Sept. 26<sup>th</sup>-Oct 1<sup>st</sup>, AIP Conf. Proceedings, 769, 1442 (2004)
- 8) S. Agostinelli et al., "GEANT4 – A simulation toolkit", Nucl. Instr. Meth. A, **506**, 250 (2003)
- 9) M. Heil et al., Nucl. Instr. Meth. A, **459**, 229 (2001)
- 10) D. Cano-Ott et al., "Neutron capture cross section measurements at n\_TOF of  $^{237}\text{Np}$ ,  $^{240}\text{Pu}$  and  $^{243}\text{Am}$  for the transmutation of nuclear waste", Proc. Int. Conf. on Capture Gamma-Ray Spectroscopy and Related Topics, CGS12, Notre Dame – Indiana, USA, Sept. 4-9, IP Conf. Proceedings, 819, 318 (2005)
- 11) N.M. Larson, "SAMMY: Multilevel R-matrix fits to neutron data using Bayes equations", ORNL/TM-9179, Oak Ridge NL, 2000